01 Oct 2018

The Rotational Spectrum and Potential Energy Surface of the Ar-SiO Complex

Michael C. McCarthy

Steve Alexandre Ndengue

Richard Dawes
Missouri University of Science and Technology, dawesr@mst.edu

Recommended Citation

M. C. McCarthy et al., "The Rotational Spectrum and Potential Energy Surface of the Ar-SiO Complex," *Journal of Chemical Physics*, vol. 149, no. 13, American Institute of Physics (AIP), Oct 2018.
The definitive version is available at https://doi.org/10.1063/1.5048202

The rotational spectrum and potential energy surface of the Ar–SiO complex

Michael C. McCarthy,[1,a)] Steve Alexandre Ndengué,[2] and Richard Dawes[2,b)]
[1]*Harvard-Smithsonian Center for Astrophysics, 60 Garden Street, Cambridge, Massachusetts 02138, USA and School of Engineering and Applied Sciences, Harvard University, 29 Oxford Street, Cambridge, Massachusetts 02138, USA*
[2]*Department of Chemistry, Missouri University of Science and Technology, Rolla, Missouri 65409, USA*

(Received 11 July 2018; accepted 6 September 2018; published online 4 October 2018)

The rotational spectra of five isotopic species of the Ar–SiO complex have been observed at high-spectral resolution between 8 and 18 GHz using chirped Fourier transform microwave spectroscopy and a discharge nozzle source; follow-up cavity measurements have extended these measurements to as high as 35 GHz. The spectrum of the normal species is dominated by an intense progression of *a*-type rotational transitions arising from increasing quanta in the Si–O stretch, in which lines up to $v = 12$ (~14 500 cm^{-1}) were identified. A structural determination by isotopic substitution and a hyperfine analysis of the Ar–$Si^{17}O$ spectrum both suggest that the complex is a highly fluxional prolate symmetric rotor with a vibrationally averaged structure between T-shaped and collinear in which the oxygen atom lies closer to argon than the silicon atom, much like Ar–CO. To complement the experimental studies, a full dimensional potential and a series of effective vibrationally averaged, two-dimensional potential energy surfaces of Ar + SiO have been computed at the CCSD(T)-F12b/CBS level of theory. The equilibrium structure of Ar–SiO is predicted to be T-shaped with a well depth of 152 cm^{-1}, but the linear geometry is also a minimum, and the potential energy surface has a long, flat channel between 140 and 180°. Because the barrier between the two wells is calculated to be small (of order 5 cm^{-1}) and well below the zero-point energy, the vibrationally averaged wavefunction is delocalized over nearly 100° of angular freedom. For this reason, Ar–SiO should exhibit large amplitude zero-point motion, in which the vibrationally excited states can be viewed as resonances with long lifetimes. Calculations of the rovibrational level pattern agree to within 2% with the transition frequencies of normal and isotopic ground state Ar–SiO, and the putative $K_a = \pm 1$ levels for Ar–^{28}SiO, suggesting that the present theoretical treatment well reproduces the salient properties of the intramolecular potential. *Published by AIP Publishing.* https://doi.org/10.1063/1.5048202

I. INTRODUCTION

The Ar–CO complex is one of the most extensively studied van der Waals (vdW) complexes,[1] because it is one of the simplest heavy atom-diatomics, and therefore can be used to provide insight into large amplitude motion, and because theoretical methods to calculate its potential energy surface (PES) and associated molecular properties are tractable. From this large body of theoretical and experimental work, Ar–CO in its ground state is known to be a very floppy, T-shaped molecule with a well depth of approximately 105 cm^{-1}[2] and to possess three very low-energy bending and stretching modes.[3] For $v_{CO} = 0$, a potential energy surface was constructed by Coudert and co-workers[4] using a global analysis of its high-resolution microwave and infrared data, and prior *ab initio* calculations. More recently, Sumiyoshi and Endo[5] determined a three-dimensional intermolecular potential energy surface by fitting 20 parameters to simultaneously reproduce nearly all of the previously reported spectroscopic data to within their experimental accuracies.

Although SiO is isovalent to CO, there are no published theoretical calculations or experimental studies on the Ar–SiO complex. Because SiO is a reactive molecule, producing it in large enough quantities to detect van der Waals complexes containing this diatomic would appear challenging, considering that complexation with an inert gas such as Ar is typically efficient at the level of 1% relative to the monomer abundance. Nevertheless, studies of complexes containing SiO may be valuable in several ways: by contributing to the comparative studies of the structure and dynamics of isovalent complexes, to investigate large amplitude motions involving a diatomic containing a second row element, and as a benchmark for theoretical treatments of the PES. Considering its nonbonded interactions, it is noteworthy that in contrast to CO which for $v = 0$ has a small dipole of about 0.1 D (oriented with the negative end on the carbon atom), SiO has a much larger dipole moment of about 3.1 D (negative end on oxygen) in $v = 0$, which increases slightly with vibrational excitation.[6,7]

Like CO, SiO has been extensively studied by calculation and various high-resolution techniques. Its rotational

[a)]Author to whom correspondence should be addressed: mccarthy@cfa.harvard.edu
[b)]dawesr@mst.edu

transitions have been observed up to $v = 46$ (~45 000 cm^{-1}) for the electronic ground state of the normal species,[8,9] and extensive measurements of its less abundant species have been made in highly vibrationally excited levels.[10,11] By combining these data with millimeter-wave spectra[12] and rovibrational measurements in the infrared,[13] a Dunham-type global analysis taking into account breakdown of the Born-Oppenheimer approximation was performed by Müller *et al.*[11] The primary motivation for much of the spectroscopic work is that radio emission lines of SiO are prominent in a number of astronomical sources, particularly stellar atmospheres,[14] and the circumstellar envelopes of evolved stars,[15,16] particularly oxygen-rich stars such as VY Canis Majoris.[17,18]

During the course of experiments to detect and structurally characterize larger silicon oxides such as the SiO_2H_2 isomers,[19] a number of strong unassigned rotational lines were observed by chirped-pulse Fourier transform (FT) microwave spectroscopy in an electrical discharge containing a dilute mixture of silane and molecular oxygen. Subsequent experiments established that the carrier for the vast majority of these lines was Ar–SiO, in which, owing to efficient vibrational excitation of SiO, each rotational transition consists of a fairly regular series of closely spaced features. A rotational analysis of these transitions was undertaken to establish if the complex is better described as a linear molecule or an asymmetric top, and to assess its rigidity.

Driven by a desire to model the interaction between Ar and SiO, we then extended our rotational analysis to include several rare isotopic species, which were observed either in natural abundance or using isotopically enriched samples. From the isotopic dependence of the rotational constants, constraints on the overall size of the complex can be set, including the distance between Ar and center of mass (CM) of the SiO subunit, and the expectation value of the angle $\Theta \equiv \angle_{(O-CM-Ar)}$, as depicted in Fig. 1. This structure is discussed in comparison to the value of Θ derived by comparing the ^{17}O quadrupole coupling constant χ_{aa} of Ar–Si^{17}O to that of free Si^{17}O and to the structures of Ar–CO and other Ar complexes.

To gain a deeper understanding of the rotational spectrum of Ar–SiO, and insight into the dynamical behavior between Ar and SiO, high-level potential energy surfaces have also been computed, in which two-dimensional surfaces were calculated for different values of the SiO stretch coordinate and, by appropriate weighting, vibrationally averaged surfaces corresponding to various quanta in SiO were produced. From these potentials, it is possible to establish the equilibrium geometry, the barrier between the linear and T-shaped geometries, and carefully examine the influence of zero-point vibration on the vibrationally averaged structure. To test the theoretical surface, computed transition frequencies were compared to those derived from experiment up to $v_{SiO} = 7$ for normal Ar–SiO, as well as $v_{SiO} = 0$ for three of the less abundant isotopic species. On the basis of these calculations, two other nearly harmonic series of lines have been tentatively assigned to $K_a = \pm 1$ levels of normal Ar–SiO in its ground vibrational state.

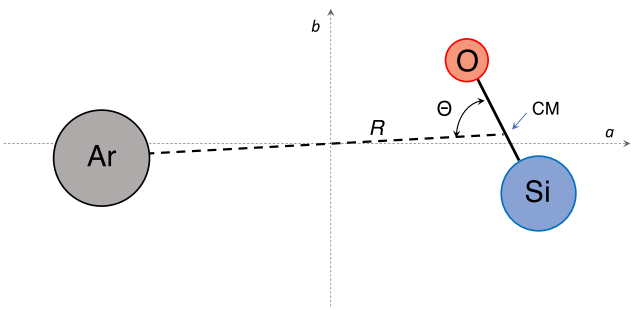

FIG. 1. Internal (Jacobi) coordinate system of Ar–SiO used in the structural determination. CM refers to the center of mass of the SiO subunit, and the Si–O bond length was constrained to the monomer value. The bond length is in Å and the bond angle is in degrees.

II. EXPERIMENTAL

A combination of chirped[20] and cavity FT microwave spectroscopies[21] was used to characterize the rotational spectra of normal and isotopic Ar–SiO. Its lines were first identified in broadband spectra acquired between 8 and 18 GHz using a spectrometer that has been described in detail elsewhere.[22,23] Following initial detection, measurements at high spectral resolution, high sensitivity, and ultimately higher frequency were performed with a cavity spectrometer operating between 5 and 26 GHz that is located in the same vacuum chamber, but along an axis perpendicular to that of the chirped spectrometer; subsequent experiments above 26 GHz were performed using a second, nearly identical cavity spectrometer,[24,25] but one that operates up to 40 GHz. In both experiments, transient species such as Si_3[26] and Si(H)SiH[27] and heavier silicon oxides such as *cis*- and *trans*-HOSiOH[19] are produced by synchronously striking an electrical discharge in the throat of a pinhole expansion as a dilute mixture of silane and oxygen (both <1%) in argon passing through an alternating set of cylindrical Torlon insulators and copper electrodes. Because the orifice size increases from 1 mm to 3 mm, and eventually to 10 mm from the faceplate of the pinhole source to the last electrode, a distance of about 4 cm, many collisions with electrons, atoms, and precursor molecules and its fragments occur prior to adiabatic expansion into the large vacuum chamber. By adjusting experimental parameters such as the precursor concentrations, discharge voltage, stagnation pressure behind the nozzle, gas pulse duration, and buffer gas, it is possible to produce a wide variety of stable and reactive molecules, ranging from closed-shell species, to radicals, and even molecular ions, sometimes in high abundance.

The discharge nozzle source is electrically isolated from the large aluminum cavity mirror on which it is mounted, but to minimize additional collisions after the last electrode, a small hole is drilled near the center of the mirror such that the nozzle sits flush with the mirror face, allowing gas to immediately expand into the chamber along the axis of the Fabry–Pérot cavity. Near the center of the chamber, corresponding either to the beam waist of the cavity or the matched microwave horns of the broadband spectrometer, the rotational temperature has dropped to a few K, and a coherent macroscopic polarization is then created by exciting with

near resonant radiation. The resulting free induction decay is detected with a sensitive microwave receiver on one of the two spectrometers.

Although the same nozzle source was used for both the cavity and chirped experiments, it is necessary in chirped operation to use a retractable, microwave absorbing curtain to block the cavity mirror opposite this nozzle, so as spoil the cavity Q, and thus avoid detecting many strong, sharp modes. Since the curtain can be inserted and retracted externally, switching between the two spectrometers only requires a few minutes.[23] Powerful and flexible in-house software is used to control, optimize, and acquire data with both spectrometers.

The presence of strong Ar–SiO lines became fairly apparent when broadband spectra using neon and argon as the buffer gas were compared. This test and other ones were performed during experiments to identify new silicon oxides such as SiO_3 and to optimize the production of the recently discovered SiO_2H_2 isomers.[19] Subsequent cavity experiments confirmed that the unassigned lines arise from one or more reactive molecules because they were not observed in the absence of the electrical discharge. The intensity of the lines is also unaltered when a small permanent magnetic is placed near the side of the chamber, strongly implying that the carrier is a closed-shell molecule. Because the lines also disappear when either silane or oxygen is removed from the gas mixture, the carrier is likely a Si- and O-bearing species, and possibly hydrogen-bearing as well. If hydrogen containing, however, the carrier must have either zero or an even number of H atoms to satisfy the requirement of a closed-shell species. Additional experiments using SiD_4 instead of SiH_4 at the same concentration yielded lines of comparable intensity, indicate that the carrier was not hydrogen-bearing. Although indirect, the microwave power which optimized the intensities of the unassigned lines in the cavity experiments was uniformly quite low, implying a highly polar molecule.

Finally, cavity tests with Ar, Ne, and Kr were performed to confirm that the unassigned lines indeed required the presence of argon. Although the strongest lines completely disappear when Ne or Ke was used instead of Ar, other lines that were observed with a good signal-to-noise ratio were still present with Ne or Kr but were significantly weaker—by more than a factor of five or more. By contrast, rotational lines of well-characterized, strongly bound species such as SiO, the various SiO_2H_2 isomers, and Si(H)SiH, are comparably intense in both Ar and Ne. Lines of the $SiH_4{-}H_2O$ complex[28] are also much weaker in Ne compared to Ar, implying the carriers for a subset of unassigned lines is probably also a complex, mostly involving one or more water molecules and an abundant small silicon oxide, perhaps either SiO, SiO_2, c-SiO_2H_2, or *cis- and trans*-HOSiOH. The D/B ratio for these lines is somewhat intermediate between that of a weakly bound complex and a tightly bound molecule.[29] Water complexes such as water-diacetylene,[30] for example, typically fall in the roughly the same D/B range because of the larger binding energy of hydrogen bound complexes compared to complexes involving a rare gas atom. (The value of $\log(D/B)$ for three comparably sized species with similar B are: −7.7 for HC_5N, −6.4 for H_2O–HC_4H, and −5.2 for Ar–HC_4H.[30–32]) Nevertheless, the most likely carrier of the strongest unassigned lines which satisfies all of the tests and chemical assays is Ar–SiO.

To determine which unassigned rotational lines in the chirped spectrum arise from the same species or vibrational state, double resonance (DR) tests were then performed with the cavity spectrometer. Such tests were generally unambiguous because it was relatively easy to saturate transitions of Ar–SiO with modest microwave power (+15 dBm), as implied from the earlier dipole moment tests. In these experiments, the cavity spectrometer was tuned to the frequency of an unassigned line, and radiation from a second synthesizer, which intersects the beam waste of the cavity, was sequentially set to the frequencies of other unassigned features. If the two rotational transitions share a common upper or low rotational level, the intensity of the cavity line normally decreases significantly in intensity owing to loss of coherence. Because it is trivial to automatically re-set the frequency of the synthesizer, and no re-tune of the cavity spacing is required, many possible binary double resonance tests can be performed automatically, and rapidly, provided the cavity line is observed with a good signal-to-noise ratio in a few seconds of integration. Once this set of tests is complete, the spectrometer is then tuned to the frequency of a second unassigned line, and the same set of double resonance tests is performed. In this way, unassigned lines can be exhaustively cross-correlated with one another in a wide band spectrum to quickly identify those that are linked together. Using this procedure, several nearly harmonic series were identified.

Under optimized experimental conditions, the ground state lines of Ar–SiO were observed with a signal-to-noise ratio of greater than 100 in 1 min of integration time with the cavity spectrometer. Line intensities decrease rapidly with increasing quanta in the Si–O stretch, but lines up to $v_{SiO} = 12$ were observed with a modest signal-to-noise ratio (~5) in 10 min of integration or less despite the large amount of vibrational energy localized in this mode (up to ~14 500 cm^{-1}). Although there is no evidence for states much above $v_{SiO} = 6$ in the chirped spectrum (Fig. 2), it was possible to detect still higher vibrational levels owing to the considerably higher detection sensitivity of the cavity spectrometer, and because the frequency spacing of vibrationally excited lines could be predicted fairly reliably for each rotational transition.

The conditions which produced the most intense signals of ground and vibrationally excited Ar–SiO were 0.1% silane and 0.1% O_2 in argon, a gas duration of 400 μs (corresponding to a flow rate of 10–15 sccm at STP), a discharge voltage of 800 V, and stagnation pressure behind the nozzle of 2.5 kTorr (3.2 atm). Strong lines of this complex were also observed when water was used in place of O_2, but because of the difficulties in precisely controlling the water concentration, owing its low vapor pressure, and because it is a residual contaminant, O_2 proved to be a more convenient and readily adjustable source of oxygen. Owing to the high yield of Ar–SiO, lines of Ar–^{29}SiO and Ar–^{30}SiO were detected in natural abundance; those of Ar–Si^{17}O were observed by replacing normal O_2 with $^{17}O_2$ (Sigma-Aldrich, >85% purity) at the same concentration, while those of Ar–Si^{18}O were observed with a statistical sample of ^{16}O/^{18}O (Sigma-Aldrich, i.e., 25% $^{16}O_2$, 50% $^{16}O^{18}O$, and $^{18}O_2$).

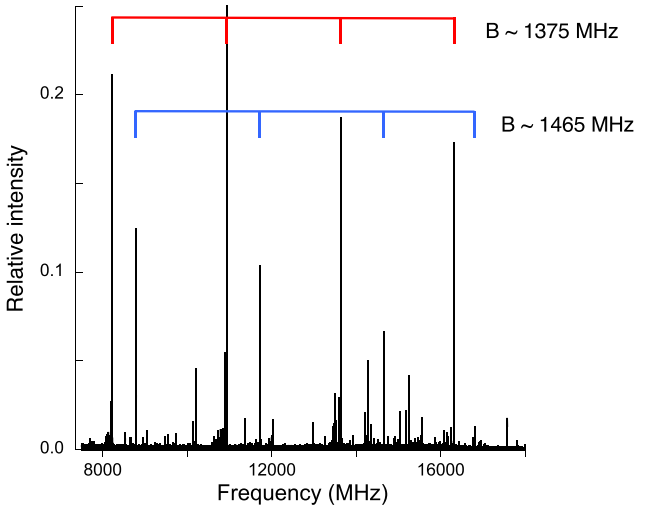

FIG. 2. Broadband spectrum between 7.5 and 18 GHz showing unassigned lines in a discharge of silane and O_2 heavily diluted in argon. Instrumental artifacts, lines of common contaminants (e.g., water dimer), silane-water complex, and silicon-bearing molecules (e.g., Si(H)SiH and Si_3) and oxides such as HOSiOH have been removed. Two progressions, one with a rotational constant of $B \sim 1375$ MHz (hereafter B1375) and another with $B \sim 1465$ MHz, dominate the spectrum. Although $B1465$ is a set of isolated features that does not require Ar, $B1375$ consists of closely spaced lines decreasing in intensity at lower frequency (see Fig. 6), all of which require the presence of Ar. Two weaker series of nearly harmonic lines with $B \sim 1421$ MHz and $B \sim 1508$ MHz are also present only with Ar. The spectrum is an average of 208 000 gas pulses, each of which was probed by 10 microwave chirps. At the 5 Hz repetition rate of the nozzle, approximately 14 h of integration was required.

III. THEORETICAL TREATMENT

A complementary theoretical study was performed in which variational rovibrational calculations were performed using a series of potential energy surfaces (PESs) representing the Ar + SiO interaction and describing a range of vibrational quanta in the SiO ($v = 0, 1, \ldots, 7$) fragment. The well depth of the Ar–SiO interaction is only -152.2 cm^{-1} at the CCSD(T)-F12b/CBS level, while the harmonic constant for SiO is 1242.03 cm^{-1},[33] which means that van der Waals (vdW) states for vibrationally excited diatom Ar–SiO ($v > 0$) complexes are resonances rather than bound states. Thus, to study the rovibrational states and their progression as a function of the number of vibrational quanta in SiO, a series of eight different 2D vibrationally averaged Ar–SiO PESs were constructed (averaged over the probability densities of the SiO vibrational states). This allows the vdW rovibrational states of interest for a particular SiO diatomic vibrational quantum number to be computed as bound states on the corresponding 2D PES (avoiding complications such as complex absorbing potentials used to compute resonances). Additional 3D calculations employing a complex absorbing potential were used to estimate the (very long) resonance lifetimes of the complex for the lowest few quanta in SiO ($v = 1$–3). First a 1D potential energy curve for SiO was computed at the CCSD(T)-F12b/CBS level and the discrete variable representation (DVR) method[34] was used to compute the $J = 0$ vibrational levels (see Table S1). The root-mean-squared error comparing the lowest 11 levels to the experimentally fitted anharmonic progression is only 1.25 cm^{-1} indicating that the employed single-reference level of theory provides a good near-equilibrium description of SiO. The Molpro electronic structure package was used for all of the calculations reported here.[35] Next, the lowest eight diatomic vibrational probability densities were represented using eight potential optimized (PO)DVR points[34] corresponding to SiO bond distances distributed between $r_{SiO} = 1.395$ and $r_{SiO} = 1.708$ Å (see Table S2).

For each of the eight SiO bond distances (PODVR points), a separate 2D Ar–SiO PES was constructed using an automated interpolating moving least squares (IMLS) method.[36–38] 400 automatically generated points were sufficient to converge the rms fitting error to on the order of 0.01 cm^{-1}. Due to the similar topography of the eight PESs, the same 2D data point locations (R, Θ, as defined in Fig. 1) were used for each value of r_{SiO}. By appropriately weighting (combining) the eight PESs according to the PODVR coefficients, PESs vibrationally averaged over the SiO (v) probability densities were obtained for Ar–SiO ($v = 0, 1, \ldots, 7$). Table S2 provides the precise PODVR point locations, as well as the relative weights given to each 2D PESs in order to construct the vibrationally averaged PESs for SiO ($v = 0, 1, \ldots, 7$). The corresponding expectation values of the r_{SiO} coordinate (used in the vdW rovibrational calculations) are also given in Table S2.

Figure 3 shows the SiO ($v = 0$) PES represented in Jacobi coordinates (see Fig. 1). As indicated in Fig. 3, strictly speaking, the global minimum ($V = -152.2$ cm^{-1}) is nearly T-shaped, but a barrier of only 7.2 cm^{-1} leads to a second minimum in a long channel along the angular coordinate. The low energy channel for SiO ($v = 0$) is only 1.4 cm^{-1} above the global minimum and extends all the way to linearity (Fig. 4). Interestingly, the relative energy of the T-shaped minimum and the channel toward linearity varies with the number of quanta in SiO (progressively favoring the more linear structure), and for SiO ($v = 7$), the T-shaped structure is no longer the global minimum. To illustrate this effect, Fig. 4 shows a

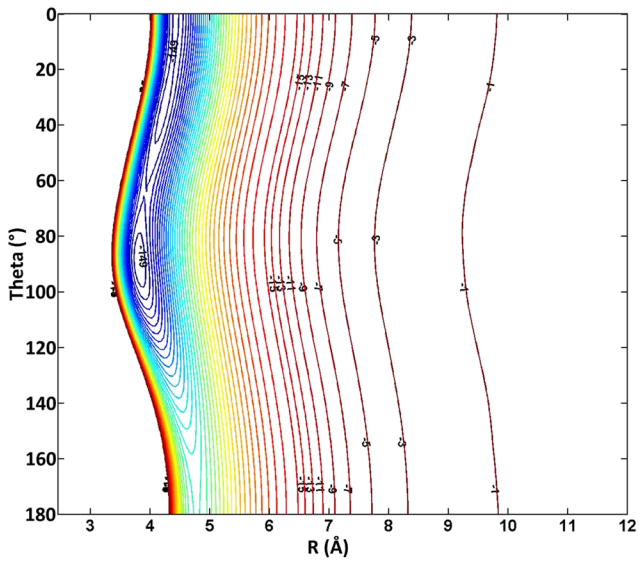

FIG. 3. Plot of the Ar–SiO ($v = 0$) interaction potential computed at the CCSD(T)-F12b/CBS level. The global minimum is roughly T-shaped, but a barrier of only 7.2 cm^{-1} leads to a long open channel only 1.4 cm^{-1} above. The contour lines are 4 cm^{-1} apart, except between 1 cm^{-1} and 15 cm^{-1} where the spacing is 2 cm^{-1}.

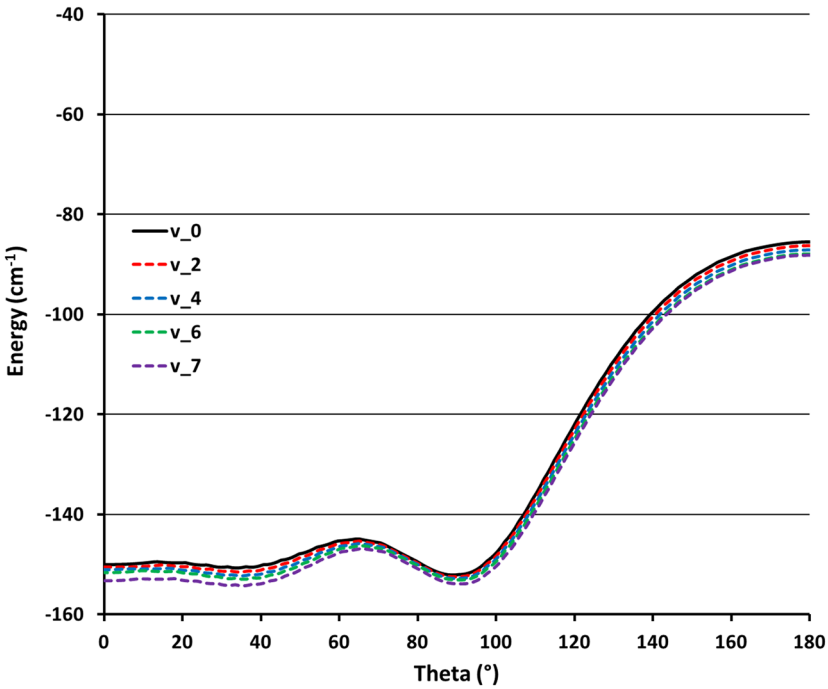

FIG. 4. The topography of the Ar–SiO ($v = n$) PES changes subtly with the SiO vibrational quantum number. The T-shaped minimum becomes progressively less stable, while the barrier and energy of the channel toward linearity become lower. This results in an increasingly linear structure and a corresponding progression of decreasing rotational constants. Here 350 cm^{-1} is taken as equal to 1 kcal/mol (strictly, cm^{-1} h c has units of energy).

minimized cut through the angle Θ for the series SiO ($v = 0$, 2, 4, 6, 7). The subtle evolution in the PES topography with the SiO vibrational quantum number dictates the progression of shifted rotational transitions measured experimentally as discussed in Sec. IV.

To compute the rovibrational levels and wavefunctions, the RV3 three-atom variational code of Wang and Carrington was used.[39] RV3 implements a parallel symmetry-adapted Lanczos algorithm and a numerically exact kinetic energy operator in various possible chosen sets of coordinates. Here we choose Jacobi coordinates for which the Hamiltonian is well known.[40] The parity-adapted rovibrational basis is a product of stretch and shared-K bend-rotation basis functions (more details have been provided previously).[41] RV3 permits specification of total angular momentum J and parity and also provides wavefunction and probability density plotting making assignment and interpretation relatively straightforward. Before performing a series of 2D calculations for SiO (v) with the set of vibrationally averaged 2D PESs, an initial 3D calculation was performed. The 3D calculation was performed with a product basis in such a way as to permit use of the eight 2D PESs, computed at different r_{SiO} bond distances (not the vibrationally averaged ones). For the r_{SiO} stretching coordinate, the same eight PODVR points were used such that the existing eight 2D PESs could be called in the 3D calculations. For the vdW stretch coordinate R, 200 sine DVR functions were used and for the angle, and the l_{max} value in the Legendre basis was set to 120 (for a total of 192 000 functions). This rather large basis converges the low-lying levels to better than 10^{-4} cm^{-1}. Low-lying (the first 10) levels for $J = 0$–10 were computed. The $J = 0$ levels are only of even parity, while both even and odd-parity levels were tabulated for $J > 0$. Wavefunctions and probability densities were computed in order to assign the states (see Fig. 5). A series of

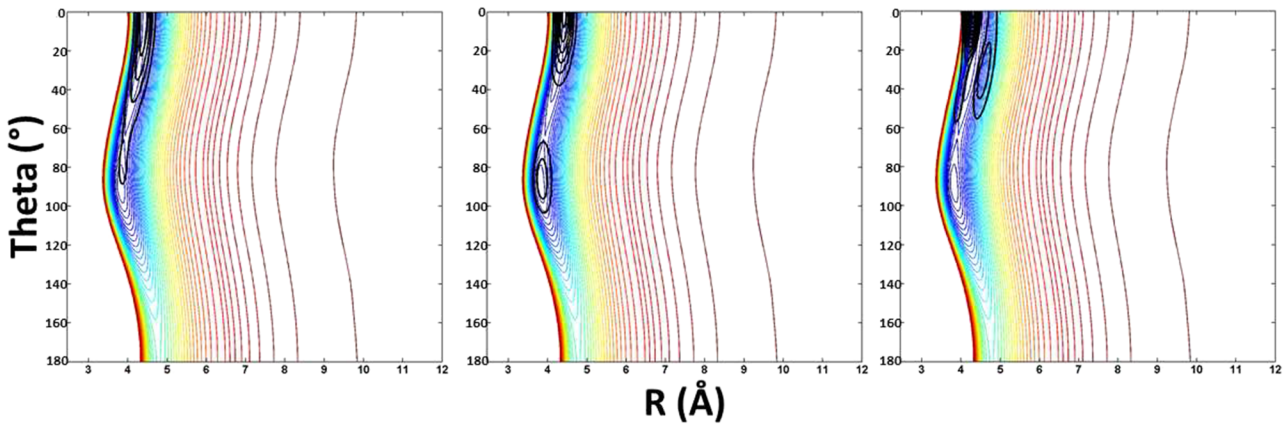

FIG. 5. Probability density plots for some $J = 0$ vdW vibrational states on the Ar–SiO ($v = 0$) PES. (Left) Ground state ($E = 0.0$ cm^{-1}), (middle) first bend-excited state ($E = 2.63$ cm^{-1}), (right) first stretch-excited state ($E = 33.57$ cm^{-1}). Probability is delocalized along a low energy channel toward linearity. The energy contour lines are 4 cm^{-1} apart, except between 1 cm^{-1} and 15 cm^{-1} where the spacing is 2 cm^{-1}.

predicted transitions were determined by considering energy differences between states which involve $\Delta J = \pm 1$ and a switch in parity.

Once the 3D results were obtained, eight separate sets of 2D calculations were performed to obtain the progression of shifts as a function of SiO (v). For each 2D calculation, r_{SiO} was fixed at the coordinate expectation value (see Table S2), and the corresponding vibrationally averaged PES was used. All of the other basis parameters were the same as in the 3D calculations. The results of the SiO (v = 0) 2D calculation are expected to be closely comparable, but not precisely the same as the full 3D calculation, and this was indeed the case. Thus, the predictions for the progressions with SiO ($v > 0$) were computed as the full $v = 0$ 3D results, shifted by the differences between the SiO (v)–SiO ($v = 0$) 2D calculations.

In addition, in order to estimate the lifetimes of the clearly long-lived resonance states observed in the experiments [those with SiO ($v > 0$)], a two-part procedure was followed. First the so-called stabilization method was used to locate the energy positions of the resonances for SiO (v = 1–3).[42] Here, the same 3D DVR procedure as was used for the bound states was employed, but with different maximum ranges of R (9.5, 12.0, 13.5, and 15.0 bohrs). With this strategy, the idea is that spurious "particle-in-a-box" states will tend to shift significantly with respect to the length of the grid, while the resonance states of interest remain relatively stable. In many applications, this approach is not favored since particularly for short-lived resonances, and the desired states also tend to shift and can be difficult to identify. In this case, however, due to the extremely long lifetimes (narrow widths) of the low-lying resonances, the stabilization procedure was rather effective. In fact, the energies of the resonances recorded for the four different grid sizes were stable to within 10^{-5} cm^{-1} and followed a similar pattern as the SiO (v = 0) levels. Next, given the precise positions, to obtain the lifetimes, an extension of the the MultiConfigurational Time-Dependent Hartree (MCTDH)-based improved relaxation method was employed[43,44] with a complex absorbing potential. This procedure has been described in detail previously.[42,45] In this case, the widths obtained for the lowest three sets of resonances, SiO (v = 1–3), are extremely narrow, less than 10^{-13} cm^{-1} (close to the numerical precision of the calculations), and corresponding to lifetimes on the order of seconds.

IV. RESULTS

A. Analysis and assignment of rotational spectra

By comparing broadband and cavity spectra under essentially identical experimental conditions, but where argon was replaced with neon, it is possible to readily identify only those spectral features which require the presence of argon, and, in turn, nearly all of which arise from normal and isotopic Ar–SiO. As indicated in Fig. 2, many such spectral features are observed with high signal-to-noise ratios. Most prominent among these are clusters of closely spaced lines separated by roughly 2.7 GHz, which were subsequently linked by DR spectroscopy, implying one or more carriers with a rotational constant of ~1375 MHz. Closer inspection reveals a similar line spacing for each cluster of lines (see Fig. 6), a pattern almost certainly arising from Ar–SiO with increasing quanta in the Si–O stretch.

Lines of Ar–^{29}SiO and Ar–^{30}SiO (v = 0) are also apparent in Fig. 6, despite the low fractional abundance of these two isotopes. In addition to the clusters of lines with $B \sim 1375$ MHz, a second series with $B \sim 1465$ MHz is also evident in the chirped spectrum in Fig. 2, and further spectroscopic analysis revealed still other series of lines displaced to higher frequency relative to the putative ground state lines. Albeit much weaker, B1465 was also observed with Ne, indicating that it cannot arise from Ar–SiO, although it has a similar rotational constant. For both Ar–Si^{17}O (v_{SiO} = 0) and Ar–Si^{18}O (v_{SiO} = 0 and 1), lines were measured in separate experiments using isotopically enriched samples of O_2. Table I summarizes lines assigned to normal, Ar–^{29}SiO, Ar–^{30}SiO, and Ar–Si^{18}O in the ground vibrational state and in

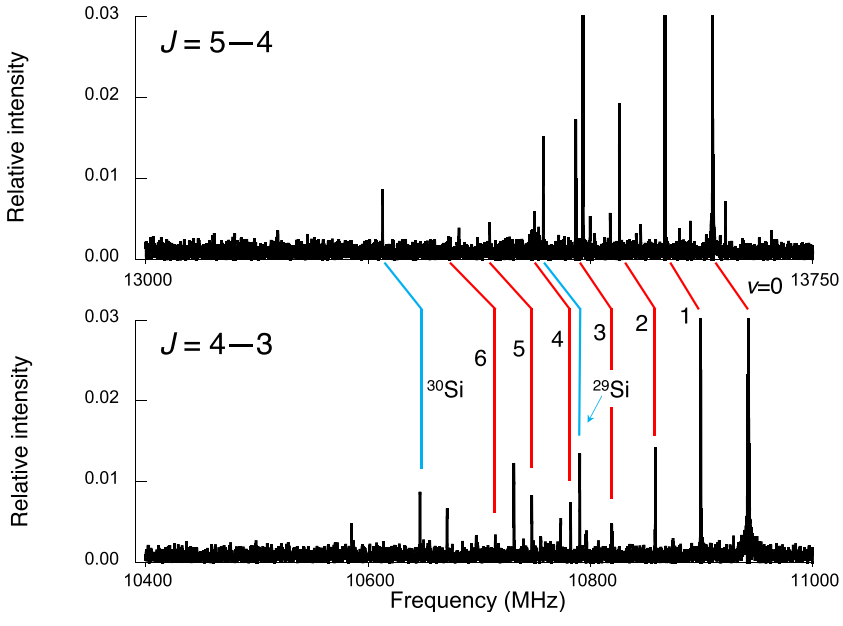

FIG. 6. Expanded view of the broadband spectrum in Fig. 2, showing two successive rotational transitions of B1375, in which the intensities of the strongest features have been truncated. A clear progression of lines is evident on this scale and arises from increasing quanta in the SiO stretch of Ar–SiO, as highlighted in red. At this signal-to-noise ratio, lines of Ar–^{29}SiO ($v = 0$) and ^{30}SiO ($v = 0$) are also observed (in blue), despite the low fractional abundance of these isotopic species, 4.7% and 3.1%, respectively.

TABLE I. Laboratory frequencies of normal and isotopic Ar–SiO in the ground state and $v_{SiO} = 1$ (in MHz).

Transition[a]	Ar–SiO		Ar–^{29}SiO		Ar–^{30}SiO		Ar–Si^{18}O	
$J'_{K'_a,K'_c} \rightarrow J_{K_a,K_c}$	GS	$v_{SiO} = 1$	GS	$v_{SiO} = 1$	GS	$v_{SiO} = 1$	GS	$v_{SiO} = 1$
$2_{0,2} \rightarrow 1_{0,1}$	5 492.794							
$3_{0,3} \rightarrow 2_{0,2}$	8 225.551	8 193.601	8 112.301		8 004.860		8 104.036	8 070.820
$4_{0,4} \rightarrow 3_{0,3}$	10 942.140	10 899.392	10 790.534	10 748.812	10 646.698	10 606.037	10 782.308	10 738.026
$5_{0,5} \rightarrow 5_{0,4}$	13 637.556	13 583.954	13 447.109	13 394.770	13 266.414	13 215.388	13 441.289	13 386.013
$6_{0,6} \rightarrow 4_{0,5}$	16 307.209	16 242.768	16 077.367		15 859.282		16 076.851	16 010.744
$7_{0,7} \rightarrow 6_{0,6}$	18 947.120	18 871.967	18 677.295		18 421.271		18 685.435	
$8_{0,8} \rightarrow 7_{0,7}$	21 554.136	21 468.561					21 264.240	
$9_{0,9} \rightarrow 8_{0,8}$	24 126.151	24 030.623					23 811.402	
$10_{0,10} \rightarrow 9_{0,9}$	26 662.267	26 557.451						
$11_{0,11} \rightarrow 10_{0,10}$	29 162.877	29 049.603						
$12_{0,12} \rightarrow 11_{0,11}$	31 629.607							
$13_{0,13} \rightarrow 12_{0,12}$	34 065.137							

[a]Estimated experimental (1σ) uncertainties are 2 kHz.

one quantum of the Si–O stretch; those arising from higher quanta in the Si–O stretch of the normal isotopic species are tabulated in Table S3. Owing to the quadrupole moment of ^{17}O ($I = 5/2$), partially resolved hyperfine structure was observed in each line of Ar–Si^{17}O (see Fig. 7). In total, 22 hyperfine components from four rotational transitions were measured (Table S4). Finally, Table S5 lists measured frequencies of two other weaker, but nearly harmonic series that also behave in the same way in chemical tests and other assays as the putative ground state lines.

The absence of K_a structure is qualitatively consistent with the rotational spectrum of a linear molecule, as opposed to that of an asymmetric top. However, attempts to fit each rotational series independently using a simple linear molecule effective Hamiltonian were unsatisfactory. For example, when the rotational constant B and two centrifugal terms (D and H) were varied in the fit of the normal species, the fit quality is poor (yielding a weighted average of 275 vs 1 for an ideal fit), and D is fairly large, of order 0.2 MHz, which is about three times larger than that reported for Ar–CO.[46] In addition, its predictive power was poor, with line frequencies of higher frequency transitions deviating by a MHz or more from those calculated. Since the J range on the measurements is quite modest ($J < 14$), the use of still higher-order distortion terms was not pursued, considering that even the sextic term H is rarely needed for well-behaved semirigid molecules at low J.

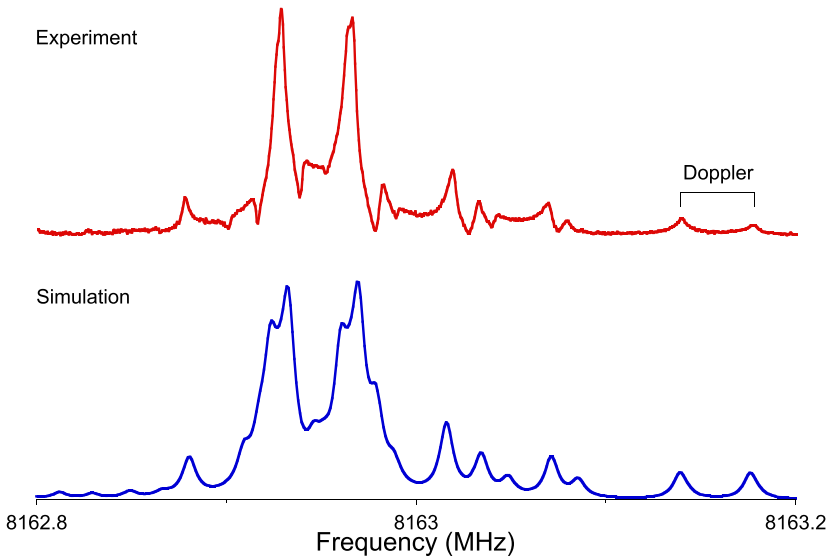

FIG. 7. The $J_{K_a,K_c} = 3_{0,3} \rightarrow 2_{0,2}$ rotational transition of Ar–Si^{17}O, showing a partially resolved hyperfine structure from the $I = 5/2$ nuclear spin of ^{17}O. Each hyperfine transition is split into two Doppler components because the supersonic jet expands along the axis of the Fabry–Pérot cavity; the rest frequency of each transition is simply the arithmetic average of these two frequencies, while the frequency separation between the doublets is proportional to the velocity of the jet. The total integration time for the experimental spectrum was approximately 1 h, and the spectral resolution was 1 kHz; the simulated spectrum has been derived from the best-fit constants listed in Table II, assuming a Doppler splitting of 36 kHz, and a Lorentzian line profile with a linewidth of 9 kHz FWHM. The observed intensities of the two strongest hyperfine features differ from the simulation owing to well-known, but systematic effects that can occur in the power spectra of closely spaced transitions.[55]

Because the linear Hamiltonian yielded unsatisfactory results, and a subsequent structural analysis by isotopic substitution indicated a geometry closer to T-shaped, the observed lines were then fit to an asymmetric top Hamiltonian with centrifugal distortion, on the assumption that they arise from the $K_a = 0$ ladder. With five free parameters, the sum and difference of the B and C rotational constants, and three centrifugal distortion terms (Δ_J, δ_J, and Φ_J), the fit yields a weighted average (1.9) comparable to the measurement uncertainty. The A rotational constant, however, is very poorly constrained from these data alone and is highly correlated (>0.97) with other parameters. Varying A by a factor of two only modestly decreases the fit quality, but negligibly impacts the effective best-fit rotational constant $(B + C)/2$, with both fits converging to essentially the same value, 1374.3 MHz. For this reason, A was constrained to 55 GHz, the value computed from the theoretical calculations in Sec. III. For consistency, we have uniformly adopted this fitting strategy in the analysis of higher-lying vibrational states and isotopic species of Ar–SiO where the experimental data are less complete. The best-fit rotational constants of Ar–SiO are given in Table II; a more complete summary of the spectroscopic constants is provided in Table S6.

As indicated in Table S7, the calculated and measured transition frequencies for the $K_a = 0$ ladder of Ar–^{28}SiO in its vibrational ground state agree to better than 2%, and comparably good agreement was achieved both for higher quanta in the Si–O stretch and for the three rare isotopic species when those calculated (Tables S8 and S9) are compared to experiment. Since the theoretical calculations well reproduced the salient features of the rotational spectrum, it was then possible to tentatively assign two other unassigned series in Fig. 2 to the low-lying $K_a = \pm 1$ ladders from theoretical predictions. For both ladders, agreement between theory and experiment appears equally good, with deviations in frequency no worse than 1.1% over the range of measurements. Although indirect, both series have comparable intensities, as might be expected for transitions that arise from levels with very similar energies above the ground state.

When both the $K_a = 0$ and putative $K_a = \pm 1$ lines are simultaneously fit using an asymmetric top Hamiltonian, a large number of higher-order centrifugal distortion constants are needed to reproduce the line frequencies. When 10 spectroscopic constants, B, C, and eight distortion terms, including octic ones such as L_{JJK}, are varied (Table S10), the fit rms is respectable (166 kHz), but still about 80 times greater than the measurement uncertainty. Varying additional distortion terms only marginally improved the fit rms, so no attempt was made to refine the fit beyond this point. With respect to the derived constants, the size of the quartic distortion constant D_{JK} (89.5 MHz) is notable. It is roughly 10 times larger than that derived for Ar–CO (9.8 MHz),[46] a clear indication of the extreme flexibility of this complex.

It should be emphasized that the semi-rigid asymmetric top model used here should be regarded as a convenient, but purely empirical fitting approach to describe a more complicated dynamical phenomenon. Despite the obvious limitations of the model, however, the effective rotational constant $(B + C)/2$ is largely insensitive to the precise fitting procedure, with differences amounting to a few 0.1% or at most a MHz for all the isotopic or vibrationally excited states studied here. Nevertheless, considerable caution should be exercised both in interpreting the other effective constants and the accuracy with which higher K_a transitions in particular can be predicted since the statistical uncertainties quoted are model dependent and are therefore almost certainly artificially small. This underlying pathology is illustrated not only by the magnitude of the quartic distortion terms, but by the slow convergence of the Hamiltonian model, i.e., the ratio $|\delta_J/\Delta_J| \sim 0.2$, while in Ar–CO, for example, the value is about 0.03.[46] As a consequence, our analysis at this juncture is somewhat more qualitative in nature, focusing specifically on how the rotational constants vary with isotopic substitution and as a function of vibrational excitation, as a means to probe the potential energy surface.

TABLE II. Effective rotational constants of normal and isotopic Ar–SiO (in MHz) derived from lines in the $K_a = 0$ ladder.

Species[a]	Vibrational state	$(B + C)/2$	$(B - C)/4$
Ar–SiO	GS	1374.3	194.8
	$v_{SiO} = 1$	1369.0	196.2
	$v_{SiO} = 2$	1364.0	195.5
	$v_{SiO} = 3$	1359.1	196.4
	$v_{SiO} = 4$	1354.5	192.7
	$v_{SiO} = 5$	1350.2	193.9
	$v_{SiO} = 6$	1346.2	186.7
	$v_{SiO} = 7$	1342.3	194.8
	$v_{SiO} = 8$	1338.9	194.8
	$v_{SiO} = 9$	1335.7	194.8
	$v_{SiO} = 10$	1332.8	194.8
	$v_{SiO} = 11$	1330.2	198.6
	$v_{SiO} = 12$	1328.0	199.4
Ar–^{29}SiO	GS	1355.5	198.6
	$v_{SiO} = 1$	1350.1	194.8
Ar–^{30}SiO	GS	1337.7	202.6
	$v_{SiO} = 1$	1332.2	194.8
Ar–Si^{17}O	GS	1363.7	195.6
Ar–Si^{18}O	GS	1353.8	187.4
	$v_{SiO} = 1$	1348.2	188.8

[a]The complete set of spectroscopic constants for each vibrational state or isotopic species is given in Table S6. Rotational constants have been rounded to the nearest tenth of a MHz.

B. Experimental structure of Ar–SiO from isotopic data

Because the effective rotational constants $(B + C)/2$ were determined for multiple isotopic species of Ar–SiO in its ground state and $v_{SiO} = 1$, it is possible to derive experimental (r_0) structures for both. In this procedure, the two unique structural parameters, the distance R between Ar and the center of mass (CM) of the SiO subunit, and the angle Θ of this subunit with respect to the line connecting Ar and the CM, as depicted in Fig. 1, were least-squares optimized to reproduce the moments of inertia of the normal, ^{29}Si, ^{30}Si, ^{17}O, and ^{18}O isotopic species. A planar structure and the one in which the Si–O bond length is unaltered by complexation were assumed. Table III lists the Si–O lengths for different vibrational states of the monomer; these in turn have been derived previously from measurements that include both Si and O rare isotopic

TABLE III. Experimental (r_0) structure of Ar–SiO in comparison to other Ar complexes.

Species[a]	Vibrational state	Si–O bond[b] length (Å)	R (Å)	Θ (deg)
Ar–SiO	GS	1.512	4.113(1)	64.3(12)
	$v_{SiO} = 1$	1.518	4.121(2)	65.0(15)
	$v_{SiO} = 2$	1.523	4.127	64.3
	$v_{SiO} = 3$	1.512	4.134	64.3
	$v_{SiO} = 4$	1.533	4.141	64.3
	$v_{SiO} = 5$	1.539	4.147	64.3
	$v_{SiO} = 6$	1.544	4.153	64.3
	$v_{SiO} = 7$	1.550	4.159	64.3
	$v_{SiO} = 8$	1.555	4.164	64.3
	$v_{SiO} = 9$	1.561	4.168	64.3
	$v_{SiO} = 10$	1.567	4.173	64.3
	$v_{SiO} = 11$	1.572	4.176	64.3
	$v_{SiO} = 12$	1.578	4.179	64.3
Ar–CO[c]		···	3.811	80(6)
Ar–N_2[d]		···	3.865	68.3
Ar–OCS[e]		···	3.699	71.9

[a]Statistical uncertainties (1σ) in the parentheses are in units of the last significant digit. For v_{SiO} = 2–12, Θ was constrained to the ground state value, and R was varied to reproduce the experimental $(B + C)/2$ rotational constant of the normal isotopic species (Table II). See Fig. 1 for an explanation of the structural parameters.
[b]Bond length fixed to the Si–O monomer for that vibrational level. See Ref. 9.
[c]Reference 46.
[d]Reference 47.
[e]Reference 48.

species. Although no isotopic data are available for $v_{SiO} = 2$ and higher states, the Ar–CM distance was optimized while constraining Θ to the ground state value because the angle is the more poorly determined parameter of the two for $v_{SiO} = 0$ and 1. Under these conditions, a slight, but fairly monotonic elongation in R is found with increasing quanta in the Si–O stretch, roughly 5 mÅ/quanta. Table III summarizes the best-fit structural parameters for states up to $v_{SiO} = 12$.

For $v_{SiO} = 0$ and 1, each structure well reproduces the effective rotational constants of the four isotopic species (i.e., to <2 MHz, or a few 0.1% for each species or vibrational state) and constrains the angle to slightly better than 3% and the distance to better than 0.1%. For Ar–CO, a similar structural analysis from isotopic data[46] yields a less certain angle (80.2° ± 6.3°), in part because C and O have similar masses, which in turn introduces some ambiguity as to which atom lies closer to Ar. Owing to the two times heavier mass of Si relative to O, and detection of two of its isotopic species, this degeneracy is lifted for Ar–SiO, yielding an angle with much improved relative precision. Although no correction was made for zero-point motion, the quality of the structural fits suggests that these effects do not change dramatically either with isotopic substitution or with at least some amount of vibrational energy in the Si–O stretch.

C. Determination of the angle Θ from Ar–Si^{17}O

An independent measure of the angle Θ in Fig. 1 can be obtained from a determination of the ^{17}O quadrupole tensor element χ_{aa} in Ar–Si^{17}O. A very similar analysis has been used in other complexes such as Ar–CO[46] and Ar–OCS,[48] so only an abbreviated description is given here. For this treatment to be valid, the electric field gradient at the ^{17}O nucleus in Si^{17}O should be unaltered by complexation, and off-diagonal elements in the quadrupole tensor should be negligible. The latter assumption might be the more tenuous of the two, but it too appears well justified, in that the ratio of $(B + C)/2A$ for Ar–SiO is both small (0.05) and comparable to that of Ar–CO (0.03). Under these conditions, the observed hyperfine pattern should then be well described by a single hyperfine term: the diagonal component of the quadrupole tensor along the a-inertial axis, χ_{aa}. In fact, the measurement of hyperfine structure in multiple rotational transitions provides a consistency check on the validity of this approximation. As indicated in Table S4, the Ar–Si^{17}O fit using just χ_{aa} well reproduces the hyperfine splitting for more than 20 partially or completely resolved components in four transitions, yielding a weighted (2.0) and fit rms (4.0 kHz) only a factor of two greater than that expected from the measurement uncertainty (2 kHz).

The quadrupole tensor element χ_{aa} is related to the monomer value eQq by rotation about the principal axis of the complex,

$$\chi_{aa} = \frac{eQq}{2}\left(3\langle\cos^2(\Theta - \phi)\rangle - 1\right), \quad (1)$$

where brackets indicate an expectation value, ϕ is the angle between the a-inertial axis and the line connecting Ar with the CM, and $eQq = 4.346(9)$ MHz has been determined previously for Si^{17}O in its ground vibrational state.[11] From the structure derived in Sec. IV B, ϕ is calculated to be quite small, 1.5°. Solving for Θ using $\chi_{aa} = 1.142(7)$ MHz (Table S4) yields two possible angles: 46° or 134°. Clearly the solution with $\Theta < 90°$ is in much better agreement with the r_0 structure, thus lending support to the argument that on average the oxygen atom lies closer than Si to the Ar atom.

The two values of Θ derived here differ by a sizable amount, about 18°. Somewhat curiously, a nearly identical variation was also found for Ar–CO,[46] in which the angle obtained from the ^{17}O hyperfine patterns was 17.9° more acute (62.3°) than that derived from the structural analysis of multiple isotopic species (80.2°). Undoubtably the wide variation of Θ in each complex is a consequence of large amplitude motion and the highly fluxional nature of these weakly bound systems.

V. DISCUSSION

In addition to Ar–SiO, Table III includes structural parameters for several other Ar complexes. Although there is a sizable scatter in the angle of the subunit with respect to Ar, this angle is also acute for Ar–SiO, in which oxygen also lies closer to the rare gas atom. However the Ar–CM distance in Ar–SiO is slightly longer, by roughly 0.3 Å or ~7%, compared to the other complexes. Since the well depth of Ar–SiO is about 50% deeper than for Ar–CO, this elongation is likely in part a consequence of the heavier mass of Si, which shifts the CM toward this atom (and hence slightly increasing the Ar–CM distance) relative to its second-row counterpart (C or N).

The present measurements indicate that there is little coupling between the Ar—CM distance and the Si–O stretching coordinate, even when large amounts of energy are localized in

this vibrational mode. On the assumption that the angle is unaltered by increasing quanta in the Si–O stretch, R increases by 0.06 Å or less than 2%, from $v = 0$ to $v = 12$, despite vibrational energy in excess of 14 500 cm^{-1} in the latter state. Because the rotational constants vary so smoothly with v, lines of even higher v_{SiO} states can probably be predicted to uncertainty of at most a few MHz near 13.5 GHz. This weak coupling is also reflected in the extremely long lifetimes (seconds) predicted by resonance calculations on the 3D potential energy surface.

In retrospect, it is perhaps not surprising that complexes of SiO are readily observed under our experimental conditions given that this species is produced so copiously from the $SiH_2 + O_2$ reaction. In analogous studies of isovalent SiS, formed from SiH_4 and H_2S, for example, it was estimated that at least 10% of the silane precursor was converted to this diatomic using a similar discharge nozzle source.[49] At this high abundance, weakly bound complexes, even if formed at the level of 1% level relative to the monomer, are likely to be readily observed. Although it is difficult to establish a precise abundance ratio between the complex and the monomer, owing to large differences in the instrumental resonse function where lines of SiO (42 GHz) and Ar–SiO (13.6 GHz) are most readily observed, we estimate that roughly 5% of SiO is found in the form of the complex. In terms of abundance per gas pulse, this percentage is equivalent to about 10^{12} clusters. With a detection sensitivity of order 10^8–10^9 molecules/gas pulse, subsequent spectroscopic analysis—as demonstrated here—can be readily extended to less abundant Si-isotopic species, and vibrationally excited states with significant energy in the Si–O stretch.

Although SiO, unlike CO, is a reactive molecule and consequently needs to be synthesized *in situ*, there are two important factors that favor detection and characterization of Ar–SiO compared to Ar–CO at centimeter wavelengths: polarity and mass. First, SiO is roughly 25 times more polar than CO (3.098 D vs. 0.1098 D; Refs. 6 and 7), and since complexation with Ar does little to alter the dipole moment (i.e., μ_a was estimated to be 0.025 D for Ar–CO; Ref. 46), lines of Ar–SiO should be far more conspicuous at the same level of abundance, since this complex is predicted to have sizable components of the dipole moment along both the a- and b-inertial axes. Because the detection sensitivity scales linearly with the dipole moment in cavity FT microwave spectroscopy, but as the square in conventional absorption, lines of Ar–SiO are greatly enhanced relative to those of Ar–CO in the latter measurements. Second, owing to the heavier mass of Ar–SiO, many rotational lines of this complex lie within the centimeter-wave band where cavity instruments are widely used. One consequence of this heavier mass is that the A rotational constant inferred from the isotopic analysis is only of order 25 GHz, compared to a value of 74 GHz for Ar–CO. For this reason, it may be possible to directly detect higher-frequency b-type transitions below the frequency ceiling of our spectrometer (~40 GHz), as opposed to millimeter-wave double-resonance experiments that were needed for Ar–CO. Furthermore, since chirped spectrometers also operate in the K_a band (26–40 GHz; Ref. 50), broadband searches may be fruitfully undertaken there, given the ease with which strong lines of this complex were observed in the C/K_u band.

It is likely that other Ar complexes containing a reactive species can be found. Those involving ions such as Ar–HCO^+[51] and radicals such Ar–OH[52] and Ar–SH,[53] for example, have previously been detected with a similar microwave spectrometer. The two most obvious candidates are Ar–CS and Ar–SiS because both diatomics can be produced in high concentration, and because they are isovalent to CO and SiO. As such, a systematic comparison of the structure and bonding of the four complexes might be worthwhile to explore how the potential energy and dynamics are altered when one or both second-row atoms are replaced with its third-row counterpart. Like Ar–SiO, rotational lines from vibrationally excited stretching modes of the diatomic will almost certainly be observed for both complexes since these are readily excited in a supersonic jet source equipped with an discharge source.[9,54] In fact, preliminary evidence for both Ar–CS and Ar–SiS has already been found in survey spectra.

SUPPLEMENTARY MATERIAL

See supplementary material for extensive tables of predicted and measured transition frequencies as well as some calculation parameters.

ACKNOWLEDGMENTS

The work in Cambridge is supported by NSF Grant Nos. CHE-1058063 and CHE-1566266. R.D. is supported by the US National Science Foundation (No. CHE-1566246).

[1] M. Havenith and G. W. Schwaab, Z. Phys. Chem. **219**, 1053 (2009).
[2] R. R. Toczyłowski and S. M. Cybulski, J. Chem. Phys. **112**, 4604 (2000).
[3] Y. Xu and A. R. W. McKellar, Mol. Phys. **88**, 859 (1996).
[4] L. H. Coudert, I. Pak, and L. Surin, J. Chem. Phys. **121**, 4691 (2004).
[5] Y. Sumiyoshi and Y. Endo, J. Chem. Phys. **142**, 024314 (2015).
[6] J. W. Raymonda, J. S. Muenter, and W. A. Klemperer, J. Chem. Phys. **52**, 3458 (1970).
[7] J. S. Muenter, J. Mol. Spectrosc. **55**, 490 (1975).
[8] R. Mollaaghababa, C. A. Gottlieb, J. M. Vrtilek, and P. Thaddeus, Astrophys. J. Lett. **368**, L19 (1991).
[9] M. E. Sanz, M. C. McCarthy, and P. Thaddeus, J. Chem. Phys. **119**, 11715 (2003).
[10] S.-H. Cho and S. Saito, Astrophys. J. Lett. **496**, L51 (1998).
[11] H. S. P. Müller, S. Spezzano, L. Bizzocchi, C. A. Gottlieb, C. Degli Esposti, and M. C. McCarthy, J. Phys. Chem. A **117**, 13843 (2013).
[12] E. Lowry Manson, W. W. Clark, F. C. De Lucia, and W. Gordy, Phys. Rev. A **15**, 223 (1977).
[13] J. M. Campbell, D. Klapstein, M. Dulick, P. F. Bernath, and L. Wallace, Astrophys. J. Suppl. Ser. **101**, 237 (1995).
[14] K. Ohnaka, Astron. Astrophys. **561**, A47 (2014).
[15] W. D. Cotton, W. Vlemmings, B. Mennesson, G. Perrin, V. Coudé du Foresto, G. Chagnon, P. J. Diamond, H. J. van Langevelde, E. Bakker, S. Ridgway, H. McAllister, W. Traub, and S. Ragland, Astron. Astrophys. **456**, 339 (2006).
[16] F. L. Schöier, D. Fong, H. Olofsson, Q. Zhang, and N. Patel, Astrophys. J. **649**, 965 (2006).
[17] M. Miyoshi, K. Matsumoto, S. Kameno, H. Takaba, and T. lwata, Nature **371**, 395 (1994).
[18] T. Kamiński, C. A. Gottlieb, K. H. Young, K. M. Menten, and N. A. Patel, Astrophys. J. Suppl. Ser. **209**, 38 (2013).
[19] M. C. McCarthy and J. Gauss, J. Phys. Chem. Lett. **7**, 1895 (2016).
[20] G. G. Brown, B. C. Dian, K. O. Douglass, S. M. Geyer, S. T. Shipman, and B. H. Pate, Rev. Sci. Instrum. **79**, 053103 (2008).
[21] T. J. Balle and W. H. Flygare, Rev. Sci. Instrum. **52**, 33 (1981).
[22] K. N. Crabtree, O. Martinez, and M. C. McCarthy, J. Phys. Chem. A **117**, 11282 (2013).

[23]K. N. Crabtree, M.-A. Martin-Drumel, G. G. Brown, S. A. Gaster, T. M. Hall, and M. C. McCarthy, J. Chem. Phys. **144**, 124201 (2016).
[24]M. C. McCarthy, M. J. Travers, A. Kovács, C. A. Gottlieb, and P. Thaddeus, Astrophys. J. Suppl. Ser. **113**, 105 (1997).
[25]M. C. McCarthy, W. Chen, M. J. Travers, and P. Thaddeus, Astrophys. J. Suppl. Ser. **129**, 611 (2000).
[26]M. C. McCarthy and P. Thaddeus, Phys. Rev. Lett. **90**, 213003 (2003).
[27]M. McCarthy and P. Thaddeus, J. Mol. Spectrosc. **222**, 248 (2003).
[28]Y. Kawashima and R. Suenram, unpublished results (2015).
[29]P. Thaddeus, M. C. McCarthy, M. J. Travers, C. A. Gottlieb, and W. Chen, Faraday Discuss. **109**, 121 (1998).
[30]K. Matsumura, F. J. Lovas, and R. D. Suenram, J. Mol. Spectrosc. **144**, 123 (1990).
[31]G. Winnewisser, M. Winnewisser, and J. J. Christiansen, Astron. Astrophys. **109**, 141 (1982).
[32]K. Matsumura, Y. Ohshima, and Y. Endo, J. Mol. Spectrosc. **185**, 178 (1997).
[33]G. Herzberg, *Molecular Spectra and Molecular Structure I. Spectra of Diatomic Molecules*, 2nd ed. (Van Nostrand Reinhold, New York, 1950).
[34]H. Wei and T. Carrington, J. Chem. Phys. **97**, 3029 (1992).
[35]H. J. Werner, P. J. Knowles, and G. Knizia *et al.*, MOLPRO, version 2012.1, a package of *ab initio* programs, 2012, see http://www.molpro.net.
[36]M. Majumder, S. A. Ndengue, and R. Dawes, Mol. Phys. **114**, 1 (2015).
[37]R. Dawes and S. A. Ndengué, Int. Rev. Phys. Chem. **35**, 441 (2016).
[38]*Reviews in Computational Chemistry*, edited by A. L. Parrill and K. B. Lipkowitz (John Wiley & Sons, Inc., 2018), Chap. 5.
[39]X.-G. Wang and T. Carrington, "RV3: A package of programs to compute rovibrational levels and wavefunctions of triatomic molecules" (unpublished).
[40]J. Tennyson, Comput. Phys. Rep. **4**, 1 (1986).
[41]S. Ndengué, R. Dawes, X.-G. Wang, T. Carrington, Jr., Z. Sun, and H. Guo, J. Chem. Phys. **144**, 074302 (2016).
[42]S. A. Ndengué, R. Dawes, F. Gatti, and H. D. Meyer, J. Phys. Chem. A **119**, 12043 (2015).
[43]*Multidimensional Quantum Dynamics: MCTDH Theory and Applications*, edited by H. D. Meyer, F. Gatti, and G. A. Worth (Wiley-VCH, Weinheim, 2009).
[44]H.-D. Meyer, F. Le Quéré, C. Léonard, and F. Gatti, Chem. Phys. **329**, 179 (2006).
[45]S. A. Ndengué, R. Dawes, and H. Guo, J. Chem. Phys. **144**, 244301 (2016).
[46]T. Ogata, W. Jäger, I. Ozier, and M. C. L. Gerry, J. Chem. Phys. **98**, 9399 (1993).
[47]W. Jäger and M. Gerry, Chem. Phys. Lett. **196**, 274 (1992).
[48]Y. Xu, W. Jäger, and M. Gerry, J. Mol. Spectrosc. **151**, 206 (1992).
[49]H. S. P. Müller, M. C. McCarthy, L. Bizzocchi, H. Gupta, S. Esser, H. Lichau, M. Caris, F. Lewen, J. Hahn, C. Degli Esposti, S. Schlemmer, and P. Thaddeus, Phys. Chem. Chem. Phys. **9**, 1579 (2007).
[50]D. P. Zaleski, J. L. Neill, M. T. Muckle, N. A. Seifert, P. B. Carroll, S. L. W. Weaver, and B. H. Pate, J. Mol. Spectrosc. **280**, 68 (2012).
[51]Y. Ohshima, Y. Sumiyoshi, and Y. Endo, J. Chem. Phys. **106**, 2977 (1997).
[52]Y. Ohshima, M. Iida, and Y. Endo, J. Chem. Phys. **95**, 7001 (1991).
[53]Y. Sumiyoshi, Y. Endo, and Y. Ohshima, J. Chem. Phys. **113**, 10121 (2000).
[54]E. Kim and S. Yamamoto, J. Mol. Spectrosc. **219**, 296 (2003).
[55]J. Haekel and H. Mäder, Z. Naturforsch., A **43**, 203 (1988).